RSC Advances

ROYAL SOCIETY OF CHEMISTRY

www.rsc.org/advances

Immobilized Polyazomethines Containing Triphenylamine Groups on ITO: Synthesis and Acidochromic, Electrochemical, Electrochromic and Photoelectronic Properties

Xiaochuan Ma[a], Yanshuang Wu[b,1], Hailin Wen[a], Haijun Niu[a]*, Cheng Wang[a], Chuanli Qin[a], Xuduo Bai[a], Lei Lei[b,*], Wen Wang[c]

a Key Laboratory of Functional Inorganic Material Chemistry, Ministry of Education, Department of Macromolecular Science and Engineering, School of Chemistry and Chemical Engineering, Heilongjiang University, Harbin 150086, P R China

b Department of Histology and Embryology, Harbin Medical University, Harbin,150081, Heilongjiang Province, China

c *School of Materials Science and Engineering, Harbin Institute of Technology, Harbin 150080, P R China*

*corresponding author, email: *haijunniu@hotmail.com; leiys2002@yahoo.com* (Lei Lei)

1. These authors contributed equally to this work

Abstract

A new series of polyazomethines (PAMs) containing triphenylamine (TPA) as easily-oxidized units were synthesized as highly soluble materials in electrochromism. The 2,5-bis(hexyloxy)terephthaldehyde and four different kinds of diamines were condensed to construct the PAMs under benign condition with $\overline{M}_n$s of 21,700 - 25,400 g/mol. Colors of the PAMs solution changed reversibly between light yellow and navy blue with the value of pH up and down. The PAMs of highly contenting alkyl groups, which could dissolve facilely in many common organic-solvents, were grafted onto ITO through siloxane linkage to cast into tough films. During the electrochemical reoxidation process, the films showed color switching with high coloration efficiency. The HOMO and LUMO levels were determined via cyclic voltammograms combined with UV-visible spectrum as -5.14 to -4.79 eV and -2.81 to -2.54 eV, respectively,

which can be utilized into hole transporting layer in organic light-emitting diodes (OLEDs) or solar cells (SCs) devices.

Keywords: Electrochromic; Triphenylamine; Siloxane; Polyazomethine

1. Introduction

Electrochromic Polymers (ECP), which can be modified conspicuously with a low-redox potential to attain a varying color state,[1] have been extensively investigated into many potential application such as smart windows,[2] electrochromic eyewear,[3] electronic paper[4] and display.[5] Among the ECP of synthetic accessibility, the modification of the main architecture which braced by multichromic monomers (e.g. pyrrole, thiophene, aniline) would pave the path to widening the electrochromes into an expansive electrochemical field.[6] Recently, amounts of noteworthy researches have focused on tuning the color into even more colorful regions. Reynolds used three colored-to-transmissive switching electrochromic polymers to blend into multicomponent ECP mixtures which cooperated to estimate the color properties.[7] Skene prepared a series of PAMs which were found to undergo oxidation program with the multichromic process from neutral to oxidized state.[8]

PAMs are interesting electrochromic materials that due to their advantageous synthesis and straightforward electronic withdrawing under facile conditions. Furthermore, the internal hybridization sp^2 of nitrogen atom in the main-chain makes the PAMs become an attractive material for electrochromic devices. This configuration has led to stronger absorption spectra in the visible origin with obvious color changes in the redox process. The other properties of PAMs such as well-documented excellent thermal, mechanical, electronic, optical, optoelectronic, and fiber forming properties also expended the additionally developing prospect.[9]

Owing to the strong electron-donating and hole-transporting/injecting properties of highly electron-rich and redox-active compounds, PAMs act as useful optic-electronic materials like xerography, light-emitting diodes, and solar cells. Among many building blocks available for constructing electrochromic polymers, rotating TPAs are unique molecules possessing particular functions such as outstanding redox activity, fluorescence and ferromagnetism.[10] They are likely to their facilely deionizing, stable oxidizability of the nitrogen atom, and transportability of positive charge centers via the radical cation species. Moreover, the propeller TPA is inclined to confer active solubility to polymers. In recent years, Hsiao has prepared new polyimides for manifesting the stable electrochromes of TPA, with a color of lightness neutral form, which switched color from red-violet/pale green reduced form to blue oxidized form.[11] Our groups have studied hole transportation and electrochromic properties of PAMs containing TPAs in OLED and electrochemical materials.[12]

However, the technological applications of most rigid PAMs are limited by processing difficulties because of the confined solubility in most organic solvents. Many approaches have been adopted to handling the problem by introducing various substituted groups, bulk monomers containing certain heterocyclic units (cardo-structure, tetraphenylethene) in the main chain,[13] and forming complex with $GaCl_3$ or β-CD.[14] Linking polymer to substrates with silicon oxide is efficiently viable route to modulate polymer layers with a terminal chain combining onto the modified surface.[15] The polymer films frequently suffer from the falling off during the electrochemical process also can adopted this strong polymer/substrate conformation to improve the electrochemical and electrochromic properties.

In the present work, we synthesized four kinds of PAMs from different TPA derivatives and discussed the effect of structure of the naphthalene and benzene group, biphenyl and phenyl group on the absorption and electrochemical properties, to acquaint how to control the energy gap by regulating structures. The introduction of naphthyl ring enhances the π-electron delocalization which significantly affects the electronic structure. And the replacement of phenyl group with biphenyl group results in the change of the space contracture and the reduction of steric hindrance. The prepared PAMs exhibited excellent solubility and well sensitive to pH. In order to prevent the PAM film peeling off, from the ITO glass, 3- triethoxy silypropylamine (APTES) was used as a bridge to connect PAMs and ITO to demonstrate stable electrochemical behavior and electrochromism of TPA-based PAM film when stimulated by electrooxidation.

2. Experimental

2.1 Materials

N,N'-di(1-naphthyl)benzidine, N,N'-di(2-naphthyl)-1,4-phenenylenediamine were bought from Qinhuangdao Bright Chemical Co. LTD; p-toluidine, N,N'-diphenyl-1,4-phenylenediamine were purchased from TCI Co.; 2,5-bis(hexyloxy)terephthaldehyde was bought from Aldrich–Sigma Co.; Pd/C (10%) was purchased from Acros; tetrahydrofuran (THF), N,N'-diphenyl-1,4-phenylenediamine (DMAc), dimethyl sulfoxide (DMSO), N,N-dimethylformamide (DMF) and toluene were supplied from Sinopharm Chemical Reagent Co. ; Lithium perchlorate ($LiClO_4$) was dried under vacuum at 120 ^oC for 36 h. N,N'-bis(4-aminophenyl)-N,N'-di(1-naphthyl)benzidine (diamine 1), N,N'-bis(4-aminophenyl)-N,N'-diphenylbenzidine (diamine 2), N,N'-bis(4-aminophenyl)-N,N'-di(2-naphthyl)-1,4-phenylenediamine (diamine 3) and

N,N'-bis(4-aminophenyl)-N,N'-diphenyl-1,4-phenylenediamine (diamine 4) were prepared by Ullman reaction according to the method described in the literatures.[16]

2.2 Synthesis of polymers

The synthesis of PAM1 was used as an example to illustrate the general synthetic procedure. To a three necked 50 ml glass reactor fitted with a magnetic stirrer, Dean-Stark trap and reflux condenser, 0.201 g (0.32×10^{-3} mol) N,N'-bis(4-aminophenyl)-N,N'-di(1-naphthyl)benzidine was dissolved in DMSO following by adding 0.112 g (0.34×10^{-3} mol) 2,5-bis(hexyloxy)terephthaldehyde under nitrogen. Then, the mixture solution of dialdehyde and diamine in 10 ml DMSO and 2 ml toluene was stirred at 120 ^{o}C for 10h. After the reaction, the obtained polymer solution was poured slowly into 200 ml of ice frozen water. The precipitate was collected by filtration, and washed thoroughly with hot methanol in a Soxhlet apparatus for 48 h, then was dried under vacuum at 70 ^{o}C overnight. Yield: 0.225 g, 75.4%, yellow.

FTIR (KBr, cm^{-1}): 1683(-HC=O), 1619 (CH=N), ^{1}H NMR (400 MHz, $CDCl_3$, ppm): 10.55 (s, -CH=O end group), 8.98-9.02 (d, -CH=N-), 7.81-8.01 (m, aromatic ring of benzene -CH=N-), 7.04-7.56 (m, aromatic ring of triphenylamine), 4.06-4.21 (m, $-OCH_2-$), 0.82-1.91 (m, methylene and terminal methyl).

The other polymers were prepared by an analogous procedure shown as Scheme 1.

Synthesis of PAM2. Yield: 0.286 g, 80.1%, yellow. FTIR (KBr, cm^{-1}): 1683 (-HC=O), 1618 (CH=N), ^{1}H NMR (400 MHz, $CDCl_3$, ppm): 10.56 (s, -HC=O end group), 9.02-9.04 (s, -CH=N-), 7.66-7.89 (m, aromatic ring of benzene -CH=N-), 7.13-7.57 (m, aromatic ring of triphenylamine), 4.03-4.23 (m, $-OCH_2-$), 0.80-1.97 (m, methylene and terminal methyl).

Synthesis of PAM3. Yield: 0.301 g, 81.6%, red. FTIR (KBr, cm^{-1}): 1682 (-HC=O), 1616 (CH=N), ^{1}H NMR (400 MHz, $CDCl_3$, ppm): 10.54 (s, -CH=O end group), 8.99-9.03 (d, -CH=N-), 7.66-7.89 (m, aromatic ring of benzene -CH=N-), 7.13-7.57 (m, aromatic ring of triphenylamine), 4.03-4.23, (m -OCH_2-), 0.82-1.93 (m, methylene and terminal methyl).

Synthesis of PAM4. Yield: 0.234 g, 74.6%, deep red. FTIR (KBr, cm^{-1}): 1682(-HC=O) 1618 (CH=N), ^{1}H NMR (400 MHz, $CDCl_3$, ppm): 10.56 (s, –HC=O end group), 8.96-9.01 (d, -CH=N-), 7.83-8.05 (m, aromatic ring of benzene -CH=N-), 6.95-7.49 (m, aromatic ring of triphenylamine), 4.03-4.16, (m –OCH_2-), 0.83-1.92 (m, methylene and terminal methyl).

Scheme.1

Scheme.1. Synthetic routes for PAM 1-4 with different diamines.

2.3 Measurements

The obtained PAMs were characterized by the following techniques: ^{1}H NMR spectra were recorded on a Bruker AC-400 MHz spectrometer in $CDCl_3$, using tetramethylsilane as an internal reference. Infrared spectra were measured on a PerkinElmer Spectrum 100 Model FT-IR spectrometer. Ultraviolet-visible (UV–vis) spectra of the polymer films were determined on a UV-3600 (Shimadzu). Thermogravimetric analysis (TGA) was conducted with a PerkinElmer Pyris 6 TGA. Experiments were carried out on about 6–8 mg powder samples heated at a heating rate of 10 ^{o}C/min in flowing nitrogen (flow rate = 10 cm^3/min). Number-average ($\bar{M}_n$) and weight-average molecular weight ($\bar{M}_w$) were performed via gel permeation chromatography (GPC) analysis on a Malvern instrument connected with one refractive index detector (Viscotek-VE3580-RI- DETECTOR) by using a polymer in THF solution at a flow rate of 1.0

ml/min at 35 ^{o}C and calibrated with polystyrene standards. Cyclic voltammetry (CV) measurements were conducted on a CH Instruments 660 A electrochemical analyzer at a scan rate of 50 mV/s in 0.1 mol/L $LiClO_4/CH_3CN$ under nitrogen atmosphere by using PAMs films being spun coating on an ITO-coated glass slide as working electrode, a Pt flake and an Ag/AgCl electrode as a counter electrode and a quasi-reference electrode respectively, and calibrated against the ferrocene /ferrocenium (Fc/Fc^+) redox couple by assuming the absolute energy level of Fc/Fc^+ as -4.80 eV to vacuum. The highest-occupied molecular orbital (HOMO) and lowest-unoccupied molecular orbital (LUMO) energy levels of the PAMs were calculated by the onsets of oxidation potentials of the films and the onsets of the maximum peak in UV-visible spectra.[17] For the electrochromic investigation, PAMs films were spun coating on ITO-coated glass slide modified by APTES and a homemade electrochemical cell was built from a commercial UV-vis cuvette. The cell was placed in the optical path of light beam in a UV-vis spectrophotometer, which allowed acquiring electronic absorption spectra under potential control under the same condition of CV determination. Scanning Electron Microscope (SEM) measurement was carried out on an S-4800 instrument with an accelerating voltage of 2 KV, and the samples were sputtered with Pt prior to observation. The morphology observation of the samples was carried out on atom force microscopy (AFM, Nanoscope IIIa digital instrument, VECCO Co.) equipped with a silicon cantilever (typical spring constant 40 N m^{-1}) in tapping mode under ambient conditions.

2.4 Preparation of the PAM films

The initially clean ITO glasses were preprocessed by dipping into the dilute potassium hydroxide solution for 30 minutes under ultrasonic concussion, washing with ethanol water and drying under nitrogen. Then they were immersed in a 5.5% (volume ratio) of APTES solution in

toluene for 40 min and washed by purified toluene. Subsequently, the monolayer substrates were formed by blowing with nitrogen gas and baking at 120 °C oven 30 min to form Si-O bonds. Next, the neat monolayers were soaked in PAMs solution to adhere the polymer onto the substrates, and then the wet glasses settled under vacuum at 100 ^{o}C for 20h (Scheme 2). According to the scheme, the structure of PAMs films were conformed directly.

Scheme 2

Scheme 2. Process of preparing PAM coated ITO electrode treated by APTES. Schematic of the structure of PAM films.

3 Results and discussion

3.1 Synthesis and characterization of polymers

The PAMs were prepared from 2,5-bis(hexyloxy)terephthaldehyde and four kinds of diamines. The PAMs was constituted through a facile one-step polycondensation under N_2 atmosphere condition. The structures of polymers were confirmed by FT-IR spectroscopy as shown in Fig S1, which indicated a strong absorption band at 1618 cm^{-1} assigned to the azomethine (C=N) stretching. Meanwhile, the ratio of monomer concentration between dialdehyde and diamine is 1.06 to 1, resulting in the appearance of carbonyl C=O stretching vibration bands at 1682 cm^{-1} attributed to end aldehyde group stretching on the main chain. In the ^{1}H NMR spectra, all the peaks could be readily assigned to hydrogen atoms in the repeating units (Fig S2). The signal at 5.0 ppm (attributed to NH_2-) disappears and a new peak at 9.0 ppm supports the formation of azomethine linkage. The proton of the aldehyde unit in terminal PAMs appear as a resonance at δ=10.56 ppm.

Propeller-like feature of TPA group enhanced the PAMs solubility behavior which was collected in Table S1. Benefiting from the long alkyl side chains connecting on the benzene unit,

all the polymers can dissolve in common organic solvents, such as THF, toluene, m-cresol. Thus, the excellent solubility makes the PAMs feasible to form high performance thin film for optoelectronic devices. The typical micromorphologies of the resulting PAMs films were characterized and analyzed by SEM and AFM in the Fig 1. Through the figures, APTES deposited on the ITO surface formed a dense and smooth thin layer on the surface of ITO (Fig 1.a and Fig 1.b). Additionally, many regular knots emerge on the surface of the APTES monolayer in the AFM image (Fig.1.e) compared to the bare ITO (Fig.1.d). PAM4 grafted onto the surface (Fig 1.c and Fig 1.f) revealed smooth and regular, which showed that APTES which was covalently bound to the ITO surface could improve the adhesive ability of polymer.

Fig. 1

Fig.1. SEM images of APTES in front (a) and in profile (b) of ITO, and PAM4 (c) on the ITO; AFM images of ITO (d), APTES in front of ITO (e) and PAM4 deposited on a silica surface (f).

3.2 Thermal properties and molecular weights

Fig. 2

Fig.2. TGA curves of PAM1 to PAM4.

The PAMs are thermally stable up to approximate 400 °C which TG analysis under nitrogen depicted in Figure 2. The PAMs exhibit good thermal stability with a 5 wt % loss at temperature of above 400 ^{o}C (Table 1) except for PAM4 which can be resulted from the less conjugated phenyl group. And the more contents of benzene in the main-chain contribute to a higher amount of carbonized residue (char yield) at 700 ^{o}C and a better thermostability. The molecular weights of PAMs were measured by GPC, using polystyrenes as standard and THF as eluent. The weight-average molecular weight ($\bar{M}_w$) and polydispersity (PDI) of PAMs were determined in the table 1, and the ($\bar{M}_w$) of PAMs was 3.62×10^4 - 2.85×10^4 (PAM1-PAM4) with PDI of 1.43-1.31,

respectively. The replacement of the phenyl group with the biphenyl ring results in the reduction of steric hindrance, which significantly increases the molecular weight.

Table 1

Table 1 Thermal properties and molecular weights of the PAMs.

3.3 Geometry and Electronic Structure of PAMs

Concerning the different structure, the optimized geometries of PAMs are shown in Figure 3. The average C-C bond length between the C=N linkage and O-phenylene in PAM1, PAM2, PAM3 and PAM4 are 1.462, 1.461, 1.461 and 1.461 Å respectively, while all that between the C=N and N-phenylene ring are 1.371 Å. The C=N bond lengths of PAMs are about 1.317Å, respectively. The azomethine bond distances are shorter than its carbon homologue resulting in part in the observed high degree of planarity. However, an obvious difference is shown on the torsional angles (Φ_1) between the C=N linkage and the adjacent N-phenylene ring in Table 2, PAM1 has a larger Φ_1 of 13.8° as compared with that (9.3°) of PAM3. The torsional angles (Φ_2) between the C=N linkage and the adjacent O-phenylene ring in PAM1 and PAM2 are 14.3° and 15.3°, respectively. The introduction of biphenyl group alter the π-stacking structure that results in large electrostatic repulsion force between the adjacent hydrogen atoms on the C=N linkage and the N-substituted benzene (H2-H3 repulsion).[18] In addition, the torsional angles (Φ_1 and Φ_2) of PAM4 are 6.7° and 11.2° which are all smaller than that of PAM3. This indicates that the naphthalene substitution significantly enhances the nonplanarity of the PAM3 backbone.[19]

Fig 3

Fig.3. Optimized geometries of PAMs.

The variation of the dihedral angles (Φ_1 and Φ_2) by the biphenyl or naphthalene substitution might result in the variant HOMO and LUMO energy levels of PAMs in the Fig 4. For the LUMO, π-conjugation of the orbital could be effectively extended across the terephthaldehyde to azomethine-phenylene cores. In contrast, the HOMO orbital shows extension of π-conjugation over azomethine and triphenylamine cores except for PAM1 which the charge separation is localized only at the terminal triphenylamine and one of the phenyl groups. The difference of the electron cloud distribution in the HOMO orbital of PAM1 may be attributed to the interruption of π-electron conjugation resulted from the introduction of the deep kink disorder of the biphenyl group.[20] It is known that the decrease of planarity lowers the HOMO level but raises the LUMO level and thus leads to a larger band gap. The calculated electronic structures (E_g) of PAM1 to PAM4 are 2.94, 3.09, 2.55 and 2.59 eV, respectively. The E_g of PAM1 and PAM3 are smaller than that of PAM2 and PAM4, respectively. This is probably accounted for naphthalene electron-withdrawing substitution. Meanwhile, the replacement of the phenyl group with the biphenyl groups aggravates the non-planarity which lowers the degree of conjugation of the PAM1 and PAM2. Thus the two conformations together change the E_g of PAMs into the order with PAM2 < PAM1 < PAM4 < PAM3.

Fig. 4

Fig.4. Pictorial representations of the electron density in the frontier molecular orbitals of repetition units.

Table 2

Table. 2. Calculated Bond Lengths, Dihedral Angles (Φ_1, Φ_2), and Electronic Structure (E_{HOMO}, E_{LUMO}, and Eg) of PAMs.

3.4 Optical properties

Fig. 5

Fig.5. UV-visible absorption spectra of PAMs in CH_2Cl_2 at room temperature.

The optical properties of the PAMs solution were investigated by UV-visible spectroscopy (Fig 5), and all the UV-vis absorption of PAMs exhibited strong absorption at 306-461 nm. The maximum absorption around 460 nm assigned to the π–π* transition resulting from the conjugation between the aromatic rings and TPA units combined by C=N double bonds in the backbone. It is observed that the PAMs containing biphenyl group have maximum peaks at shorter site than those containing 1,4- phenyl group, as it is: $\lambda_{PAM1} = \lambda_{PAM2} < \lambda_{PAM3} = \lambda_{PAM4}$. This is due to the tiny difference of dihedral angle between biphenyl and phenyl group substituted which $\Phi_{PAM1} > \Phi_{PAM3}$ and $\Phi_{PAM2} > \Phi_{PAM4}$. Whereas, the absorption maxima of PAM3 are same to that of PAM4 due to the replacement of the benzene ring with the naphthalene ring enhances the degree of the conjugation and the π-electron delocalization. From the Fig S3, small increases in the absorption maxima from solution to thin films for all PAMs. The band gaps of the polymer films obtained from the optical absorption edge are in the range of 2.25-2.33 eV, which are lower than the theoretical results. It can be regard as that the increase in absorption maximum almost derived from increased planarity of the chain in the solid state.

3.5 Acidochromic properties

Fig. 6

Fig.6. UV-vis spectra changes of PAM2 in the CH_2Cl_2 as they were protonated by HCl vapor in steps decrease with the value of pH decreasing. The concentration of pure PAMs was 0.03 mg/L. Inset photographs indicated the color evolved in the process of doping HCl vapor. The undoped molecular structure and protonated extreme resonance forms of PAMs shown on right.

As shown in the spectra (Fig.6), after doping HCl vapor the new absorption bands emerged at 591 nm. At the moment, the absorption maxima (451 nm) of PAM2 are going steadily downhill. With the acidity strengthening, the value of pH is decreasing from 6.60 to 4.50, the color of the solution deepens from the original yellow to protonated blue. The present isobestic point in absorption spectra of PAM2 confirms the coexistence of different forms of compound. While after neutralizing acidic solution, by NH_3 vapor, the color of solution turned back. The similar color changes of other PAMs are showed in Fig S4.

Because of the conjugation of the three phenyl rings in the TPA, the lone pair electron of central nitrogen would delocalize on the whole TPA which will weaken the activity of the lone pair electron to acid. The color change after being protonated by hydrochloricacid vapor would attribute to the nitrogen atom in the imine linkage (-HC=N-) doped with H^+ rather than the nitrogen in the TPA core, which single triphenylamine (TPA) was used as an illustration shown in the Fig S5 (single TPA solution was doped by concentrated sulfuric acid with a color change from lightness to blue and concentrated hydrochloric acid without switching color). Nitrogen atom in the C=N doped by acid resulted in the creation a positive charge and a stable conformation with the chloride anion. The new-form contracture increased π-electron delocalization and confirmed a much stronger electron-accepting center. Because of this, the charge separation of π-electrons in the PAMs with donor-acceptor structure accelerated electron cloud overlap and reduced the band gap. Moreover, after NH_3 vapor undoping, the changed one restores former constitution. To sum up, PAMs reveal noteworthy acidochromic properties and especially sensitive to pH value.

3.6 Electrochemical properties

Fig. 7

Fig.7. Cyclic voltammetry for PAMs in CH_3CN containing 0.1mol/L $LiClO_4$, at a scan rate of 50 mV/s.

The electrochemical properties of these PAMs films which cast on an ITO-coated glass substrate as working electrode were conducted by CV (Fig. 7), and the whole test procedures were proceed in dry acetonitrile under nitrogen atmosphere. The CV diagrams of PAM1 and PAM2 demonstrated oxidative and reductive peaks at (1.06, 0.97 V) and (0.62, 0.82 V), respectively. The difference between PAM1 and PAM2 can be attributed to the stronger conjugated structure of substituent naphthalene group. One pair of redox peaks of PAM1 and PAM2 are attributed to the lack or absence of electrochemical splitting, neither electrostatic effects nor electron coupling with oxidation of the electron-rich nitrogen atom in the TPA core. On the contrary, PAM3 and PAM4 exhibited similar two couples of symmetrical redox waves, in which the oxidative peaks at 0.79 and 1.13 V (PAM3), 0.75 and 1.05 V (PAM4) vs Ag/AgCl, respectively; the reductive peaks at 0.67, 0.96 V (PAM3) and 0.60, 0.85 V (PAM4) vs Ag/AgCl, respectively. The first oxidative peaks of PAM3 and PAM4 are attributed to the oxidation of one of N atoms in the TPA cores; the second ones resulted from a dication structure formed from radical recombination.[21]

The HOMO and LUMO energy levels of the polymer can be determined from the oxidation onset potentials of CV, and the electronic structure parameters of PAMs are given in Table 3. When the benzene ring (PAM2 and PAM4) in the side chain was replaced by the naphthalene (PAM1 and PAM3) unit, the E_g decreased only slightly. The E_g of PAM1 and PAM2 was larger than those of PAM3 and PAM4, which is attributed to the interruption of the linearity of the conjugated backbone.

Table 3

Table 3. Optical and electrochemical properties for PAMs

3.7 Electrochromic properties

Fig. 8

Fig.8. Electronic absorption spectra of films of PAM1 (a) and PAM3 (b) and their 3D spectra respectively, in the process of electrochemical doping with 0.1 V potential intervals in CH_3CN containing 0.1mol/L $LiClO_4$ as the supporting electrolyte (vs Ag/AgCl).

The excellent solubility could enhance the processibility of PAMs, but it also can be a threat to the stability of PAM film in the electrochemical redox process. Thereby, in the electrochemical treatments, the polymer films were tailored to graft onto ITO surface by siloxane linkages.

The electrochromic absorption spectra were monitored with a UV–vis spectrometer at different applied potentials. The typical electrochromic absorption spectra of PAM1 and PAM3 are showed in Fig 8, and electrochromic absorption spectra of other PAMs are showed in Fig S6. The absorption of PAM1 started to change at 470 nm in which characteristic of π-π* transition happened in TPA group at 1.2 V. When the applied potentials increased positively from 1.2 to 1.9 V, the characteristic absorbance peak at 470 nm decreased gradually, and one new band grew at 602 nm with the color changed from yellow to blue due to the electron oxidation. However the absorption of PAM3 showed varying process resulted from the different oxidation process. When the applied potential was added to 1.0 V, new bands grew up at 986 nm gradually with the color changed to green. And with potential increasing to 1.7, the absorption at 470 nm of PAM3 faded away and the other new peaks climbed at 1144 nm with color changed to blue. This alternative absorption can be attributed to the step-by-step formation of dication in the PAM segments by the further oxidation of monocation radical species.

Fig. 9

Fig.9. Electrochromic device of PAM2 containing 0.5mol/L $LiClO_4$ as the supporting electrolyte in the neutral (left) and oxidated (right) states.

Since the PAMs showed well color changes during oxidation processes, PAM2 was chosen to fabricate an electrochromic device which showed remarkable electrochromic properties (shown in Fig 9).

Fig. 10

Fig.10. Potential step absorptiometry (A) and current consumption (B) of PAM1 at 602 nm (in 0.1 mol/L $LiClO_4/CH_3CN$) by applying a potential step (0.0-1.0 V) with a cycle time of 10 s.

The response time and coloration efficiency upon electrochromic switching of the polymer film from its neutral to oxidized forms was monitored Fig 10. For reaching 90% of the full change in absorbance, the required switching time is calculated. PAM1 would require 3.0 s at 1.0 V for switching transmittance at 602 nm and 3.0 s for bleaching. After continuous cyclic scans between 0.0 V and 1.0V in 100 cycles (Fig.10B), the polymer films still exhibited good stability of electrochromic characteristics, indicating that the film was stable and had good adhesion on the ITO substrate. Through the Table 4, we can conclude that the coloration efficiency (η) of PAMs are in the order of PAM4 (332)> PAM1 (208)> PAM2 (172)> PAM3 (78). The difference of coloration efficiency may be attributed to the combination of the electron transportation along the PAM main chain and the ions transferability of the PAMs supermolecular assembly on the ITO. The replacement of phenyl group with the biphenyl and naphthyl ring improved the conjugation of the PAMs chain which may enhance the electron or hole transferability from PAM4 to PAM1. While the ions transfer also can be affected by the aggregation of PAM chains. The larger twisting

biphenyl and higher steric hindrance of naphthyl may impel PAM chain to depart with longer distance from the other which posed an aggravated effect for ions transfer between interchains. The combination of the two aspects of effect contributed the highest coloration efficiency of PAM4 and lowest one of PAM3. The coloration efficiency of PAM4 film exhibits up to 332 cm^2/C at 602 nm and shows highly stable electrochromism.

Table 4

Table 4 Electrochemical data collected for coloration efficiency measurements of PAMs.

3.8 Photoelectrical properties

Fig. 11

Fig.11. A typical photocurrent (lower) and photovoltaic (upper) response for an PAM1 film immobilized on ITO glass upon exposure to light with switching at room temperature.

Besides the stably and notably electrochemical performance, a reversible rise/decay of the photocurrent and photovoltaic were observed when light switching on and off many times, as shown in Fig.11. The measurement was tested in 0.1mol/L $LiClO_4$ electrolyte solution via a simple way which illuminated by 500W Xe arc lamp under white light of 150 mW/cm^2 intensity. Upon irradiation, the photocurrent increased and rapidly reached an approximately steady-state value of 2.4×10^{-6} A. When the light been off, the current slump dramatically to the original state. Otherwise, the excited current density decreased slightly after several on/off cycles. This indicated PAM1 have stable response to light and reversible change under being photoinduced, the similar trend as other PAMs (Fig. S7). It has been known that the photo-generated electrons transported from the lowest unoccupied molecular orbital to the conduction band on the ITO surface, and then moved to the external circuit. The photocurrent and open-circuit photovoltaic were generated among the particulate hopping of electrons. A similar characteristic was observed for other PAMs

of this series. Thus, these PAMs could be used as the photoelectric conversion material for optoelectronic application.

4. Conclusions

A series of highly soluble electrochromic polymers with excellent optical transmittance change have been synthesized from dialdehyde and four TPA derivatives. The good solubility in many organic solvents such as THF, $CHCl_3$, DMF and DMAc is beneficial for polymer film formation. An obvious color change was observed from yellow neutral form to blue after doping with acids vapor. The PAMs immobilized onto ITO via siloxane linkage (APTES) exhibit excellent reversible electrochemical behavior and continuous cyclic stability of electrochromic characteristics. The color of PAMs could be varied from initial yellow to blue via electrooxidation. Thus, these PAMs can be used in electrochromic and optoelectronic devices and sensors for pH.

Acknowledgements

The authors are grateful to the support of the National Science Foundation of China (Grant No.51373049, 51372055, 51303045, 51273056, 21372067), Doctoral Fund of Ministry of Education of China (20132301120004, 20132301110001).

References

[1] (a) G. Gunsbas and L. Toppare, *Chem. Commun.*, 2012, 48, 1083-1101; (b) J.A. Kerszulis, K.E. Johnson, M. Kuepfert, D. Khoshabo, A. L. Dyer and J. R. Reynolds, *J. Mater. Chem. C*, 2015, 3, 3211-3218; (c) L.C. Lin, H.J. Yen, Y.R. Kung, C.M. Leu, T.M. Lee and G.S. Liou, *J. Mater. Chem. C*, 2014, 2, 7796-7803; (d) S. O. Hacioglu, S. Toksabay, M. Sendur and L. Toppare, *J. Polym. Sci., Part A: Polym. Chem.*, 2014, 52, 537-544.

[2] (a) H. W. Heuer, R. Wehrmann and S. Kirchmeyer, *Adv. Funct. Mater.*, 2002, 12, 89-94; (b) S.M. Wang, L. Liu, W.L. Chen and E.B. Wang, *Electrochim. Acta*, 2013, 113, 240-247; (c) X.M. Chen, H.L. Liu, Z.P. Xu, S. Mi, J.M. Zheng, and C.Y. Xu, ACS *Appl. Mater. Interfaces*, 2015, 7, 11387-11392.

[3] A.M. Österholm, E. Shen, J.A. Kerszulis, R.H. Bulloch, M. Kuepfert, A.L. Dyer, and J.R. Reynolds, ACS *Appl. Mater. Interfaces*, 2015, 7, 1413-1421.

[4] (a) A. Malti , E.O. Gabrielsson , X. Crispin and M. Berggren, *Adv. Mater.*, 2015, 27, 3909-3914; (b) J. Matsui, R. Kikuchi, and T. Miyashita, *J. Am. Chem. Soc.*, 2014, 136, 842-845.

[5] (a) P. Tehrani, L.O. Hennerdal, A.L. Dyer, J. R. Reynolds and M. Berggren, *J. Mater. Chem.*, 2009, 19, 1799-1802; (b) H.C. Moon, T.P. Lodge and C.D. Frisbie, *Chem. Mater.*, 2015, 27, 1420-1425; (c) R.J. Mortimer, A.L. Dyer and J.R. Reynolds, *Displays*, 2006, 27, 2-18.

[6] (a) P. Camurlu, *RSC Adv.*, 2014, 4, 55832-55845; (b) D.E. Shen, L.A. Estrada, A.M. Österholm, D. H. Salazar, A.L. Dyer and J.R. Reynolds, *J. Mater. Chem. A*, 2014, 2, 7509-7516; (c) N. Guven and P. Camurlu, *Polymer*, 2015, 73, 122-130; (d) A Bolduc and W.G. Skene, *Polym. Chem.*, 2014, 5, 1119-1123. (e) Y.W. Chuang, H.J. Yen and G.S. Liou, *Chem. Commun.*, 2013, 49, 9812-9814; (f) H.J. Yen and G.S. Liou, *Chem. Commun.*, 2013, 49, 9797-9799.

[7] R.H. Bulloch, J.A. Kerszulis, A.L. Dyer, and J.R. Reynolds, ACS *Appl. Mater. Interfaces*, 2015, 7, 1406-1412

[8] M.E. Mulholland, D. Navarathne, M.L. Petrus, T.J. Dingemans and W.G. Skene, *J. Mater. Chem. C*, 2014, 2, 9099-9108,

[9] (a) A. Iwan, B. Boharewicz, K. Parafiniuk, I. Tazbir, L. Gorecki, A. Sikora, M. Filapek and E.S. Balcerzak, *Synth. Met.*, 2014, 195, 341-349; (b) J.C. Chen, Y.C. Liu, J.J. Ju, C.J. Chiang and Y.T.

Chern, *Polymer*, 2011, 52, 954-964; (c) A. Bolduc, S. Dufresne and W.G. Skene, *J. Mater. Chem.*, 2012, 22, 5053-5064; (d) D. Sek, A. Iwan, B. Jarzabek, B. Kaczmarczyk, J. Kasperczyk, Z. Mazurak, M. Domanski, K. Karon and M. Lapkowski, *Macromolecules*, 2008, 41, 6653-6663.

[10] (a) W.H. Chen, K.L. Wang, D.J. Liaw, K.R. Lee and J.Y. Lai, *Macromolecules*, 2010, 43, 2236-2243; (b) Y.C. Hu, C.J. Chen, H.J. Yen, K.Y. Lin, J.M. Yeh, W.C. Chen and G.S. Liou, *J. Mater. Chem.*, 2012, 22, 20394-20402; (c) S.H. Hsiao and Y.T. Chou, *Polymer*, 2014, 55, 2411-2421; (d) W.H. Chen, K.L. Wang, W.Y. Hung, J.C. Jiang, D.J. Liaw, K.R. Lee, J.Y. Lai and C.L. Chen, *J. Polym. Sci. Polym. Chem.*, 2010, 48, 4654-4667.

[11] H.M. Wang and S.H. Hsiao, *J. Mater. Chem. C*, 2014, 2, 1553-1564.

[12] (a) J.W. Cai, P. Zhao, H.J. Niu, Y.F. Lian, C. Wang, X.D. Bai and W. Wang, *Polym. Chem.*, 2013, 4, 1183-1192; (b) H.J. Niu, P.H. Luo, M.L. Zhang, L. Zhang, L.N. Hao, J. Luo, X.D. Bai and W. Wang, *Eur. Polym. J.*, 2009, 45, 3058-3071.

[13] (a) Y. Zhu, R.D. Champion and S.A. Jenekhe, *Macromolecules*, 2006, 39, 8712-8719; (b) C.J. Yang and S.A. Jenekhe, *Macromolecules*, 1995, 28, 1180-1196; (c) X.D. Zhuang, Y. Chen, B.X. Li, D.G. Ma, B. Zhang and Y.X. Li, *Chem. Mater.*, 2010, 22, 4455-4461.

[14] (a) C.J. Yang, S.A. Jenekhe, S.J. Meth and H. Vanherzeele, *Polym. Adv. Technol.*, 1994, 5, 161-170; (b) Y. Liu, Y.L. Zhao, H.Y. Zhang, X.Y. Li, P. Liang, X.Z. Zhang and J.J. Xu, *Macromolecules*, 2004, 37, 6362-6369.

[15] (a) N. Marshall, S.K. Sontag and Jason Locklin, *Macromolecules*, 2010, 43, 2137-2144; (b) F. Alonso, I.P. Beletskaya and M. Yus, *Tetrahedron*, 2008, 64, 3047-3101; (c) G.M. Liu and G.Z. Zhang, *J. Phys. Chem. B*. 2005, 109, 743-747; (d) O. Borozenko, C. Ou, W.G. Skene and S.

Giasson, *Polym. Chem.*, 2014, 5, 2242-2252; (e) G. Zotti, A. Randi, S. Destri, W. Porzio and G. Schiavon, *Chem. Mater.*, 2002, 14, 4550-4557.

[16] (a) H.J. Niu, Y.d. Huang, X.d. Bai, X. Lia and G.L. Zhang, *Mater. Chem. Phys.*, 2004, 86, 33-37; (b) H.J. Niu, J.W. Cai, P. Zhao, C. Wang, X.D. Bai and W. Wang, *Dyes. Pigments.*, 2013, 96, 158-169; (c) Y.F. Wang, T.M. Chen, K. Okada, M. Vekawa, T. Nakaya and M. Kitamura, *J. Polym. Sci. Polym. Chem.*, 2000, 38, 2032-2040; (d) G.S. Liou and S.H. Hsiao, *J. Polym. Sci. Polym. Chem.*, 2003, 41, 94-105.

[17] C.H. Duan, W.Z. Cai, F. Huang, J. Zhang, M. Wang, T.B. Yang, C.M. Zhong, X. Gong and Y. Cao, *Macromolecules*, 2010, 43, 5262-5268.

[18] C.L. Liu and W.C. Chen, *Macromol. Chem. Phys.*, 2005, 206, 2212-2222.

[19] F.C. Tsai, C.C. Chang, C.L. Liu, W.C. Chen and S.A. Jenekhe, *Macromolecules*, 2005, 38, 1958-1966.

[20] (a) B. Liu, W.L. Yu, Y. H. Lai and W. Huang. *Chem. Mater.*, 2001, 13, 1984-1991; (b) C.J. Xia and R. C. Advincula, *Macromolecules*, 2001, 34, 5854-5859.

[21] X.C. Ma, H.J. Niu, H.L. Wen, S.H. Wang, Y.F. Lian, X.K. Jiang, C. Wang, X.D. Bai and W. Wang, *J. Mater. Chem. C*, 2015, 3, 3482-3493.

Captions

Scheme.1. Synthetic routes for PAM 1-4 with different diamines.

Scheme.2. Process of preparing PAM coated ITO electrode treated by APTES. Schematic of the structure of PAMs film.

Fig.S1. FT-IR spectra of PAM1 to PAM4.

Fig.S2. ^{1}H NMR spectra of PAM1 to PAM4.

Table.S1. Solubility of PAMs

Fig.1. SEM images of APTES in front (a) and in profile (b) of ITO, and PAM4 (c) on the ITO; AFM images of ITO (d), APTES in front of ITO (e) and PAM4 deposited on a silica surface (f).

Fig.2. TGA curves of PAM1 to PAM4.

Table.1. Thermal properties and molecular weights of the PAMs.

Fig.3. Optimized geometries of PAMs.

Fig.4. Pictorial representations of the electron density in the frontier molecular orbitals of repetition units

Table. 2. Calculated Bond Lengths, Dihedral Angles (Φ_1, Φ_2), and Electronic Structure (E_{HOMO}, E_{LUMO}, and E_g) of PAMs.

Fig.5. UV-visible absorption spectra of PAMs in CH_2Cl_2 at room temperature.

Fig.S3. UV-visible absorption spectra of PAMs in solid state at room temperature.

Fig.6. UV-vis spectra changes of PAM2 and PAM3 in the CH_2Cl_2 as they were protonated by HCl vapor in steps decrease with the value of pH decreasing. The concentration of pure PAMs was 0.03 mg/L. Inset photographs indicated the color evolved in the process of doping HCl vapor. The undoped molecular structure and protonated extreme resonance forms of PAMs shown on right.

Fig. S4. UV-vis spectra changes of PAM1 and PAM4 in the CH_2Cl_2 as they were protonated by HCl vapor in steps decrease with the value of pH decreasing.

Fig. S5. UV-vis spectra changes of TPA as a reference in the CH_2Cl_2, concentrated sulfuric acid/ CH_2Cl_2 and concentrated hydrochloric acid/ CH_2Cl_2 solutions. Inset: the color change of TPA in the CH_2Cl_2 solution containing different proportional sulfuric and hydrochloric acid. TPA can be

protonated by the concentrated sulfuric acid to blue color state and not showed any color change from doping with concentrated hydrochloric acid.

Fig.7. Cyclic voltammetry for PAMs in CH_3CN containing 0.1mol/L $LiClO_4$, at a scan rate of 50 mV/s.

Table 3. Optical and electrochemical properties for PAMs.

Fig.8. Electronic absorption spectra of films of PAM1 (a) and PAM3 (b) and their 3D spectra respectively, in the process of electrochemical doping with 0.1 V potential intervals in CH_3CN containing 0.1mol/L $LiClO_4$ as the supporting electrolyte (vs Ag/AgCl).

Fig.S6. Electronic absorption spectra of films of PAM2 and PAM4 in the process of electrochemical doping with 0.1 V potential intervals in CH_3CN.

Fig.9. Electrochromic device of PAM2 containing 0.5mol/L $LiClO_4$ as the supporting electrolyte in the neutral (left) and oxidated (right) states.

Fig.10. Potential step absorptiometry (A) and current consumption (B) of PAM1 at 602 nm (in 0.1 mol/L $LiClO_4$/CH_3CN) by applying a potential step (0.0-1.0 V) with a cycle time of 10 s.

Table 4 Electrochemical data collected for coloration efficiency measurements of PAMs.

Fig.11. A typical photocurrent (lower) and photovoltaic (upper) response for an PAM1 film immobilized on ITO glass upon exposure to light with switching at room temperature.

Fig.S7. The typical photocurrent (lower) and photovoltaic (upper) response for an PAM2, PAM3 and PAM4 films immobilized on ITO glass upon exposure to light with switching at room temperature.

Scheme.1

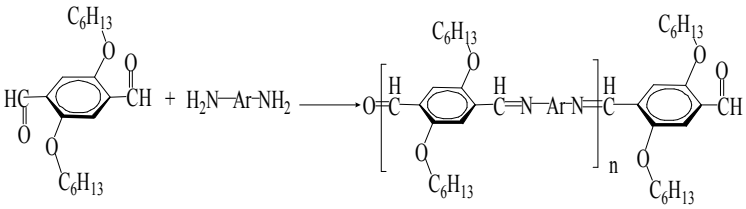

Ar=

1 2 3 4

Scheme.1. Synthetic routes for PAM 1-4 with different diamines.

Scheme 2

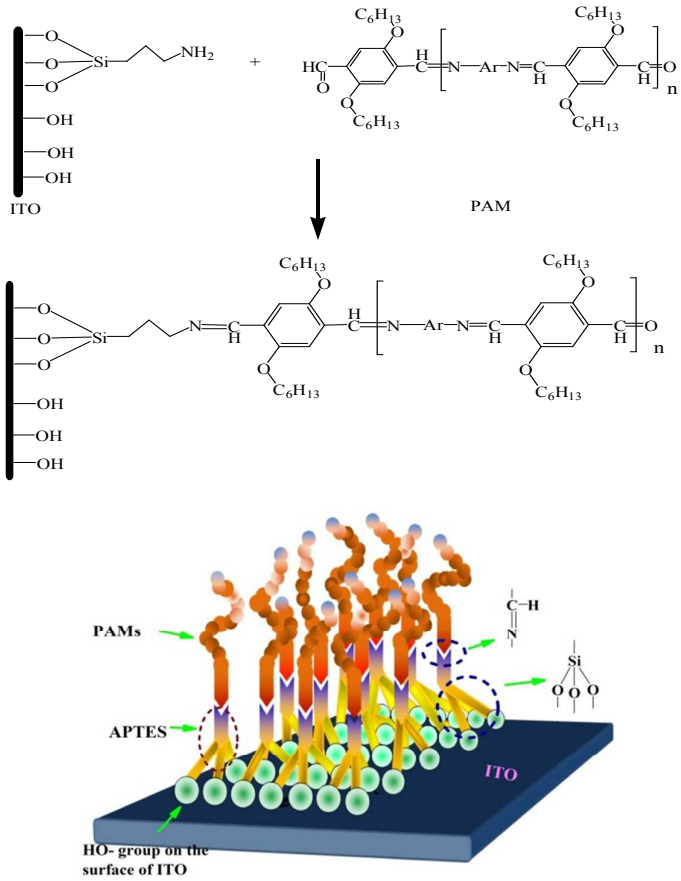

Scheme 2. Process of preparing PAM coated ITO electrode treated by APTES. Schematic of the structure of PAMs film.

Fig. 1

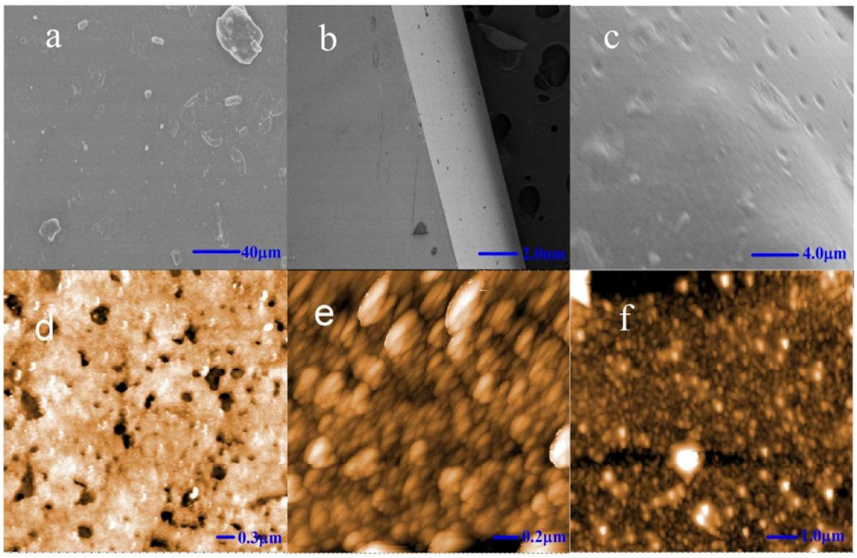

Fig.1. SEM images of APTES in front (a) and in profile (b) of ITO, and PAM4 (c) on the ITO; AFM images of ITO (d), APTES in front of ITO (e) and PAM4 deposited on a silica surface (f).

Fig. 2

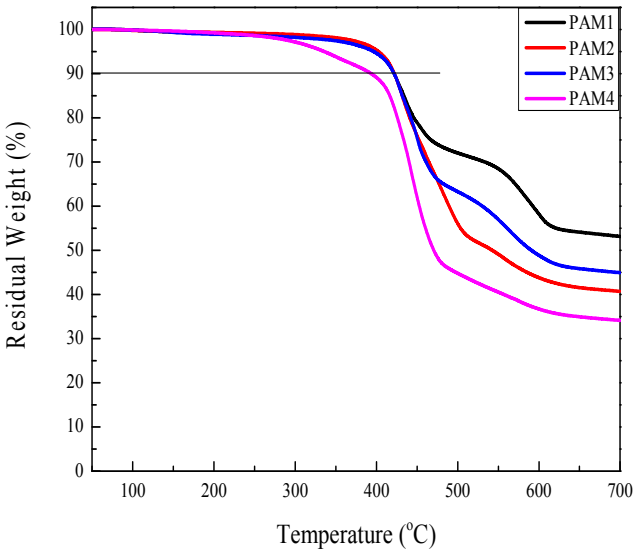

Fig.2. TGA curves of PAM1 to PAM4.

Fig 3

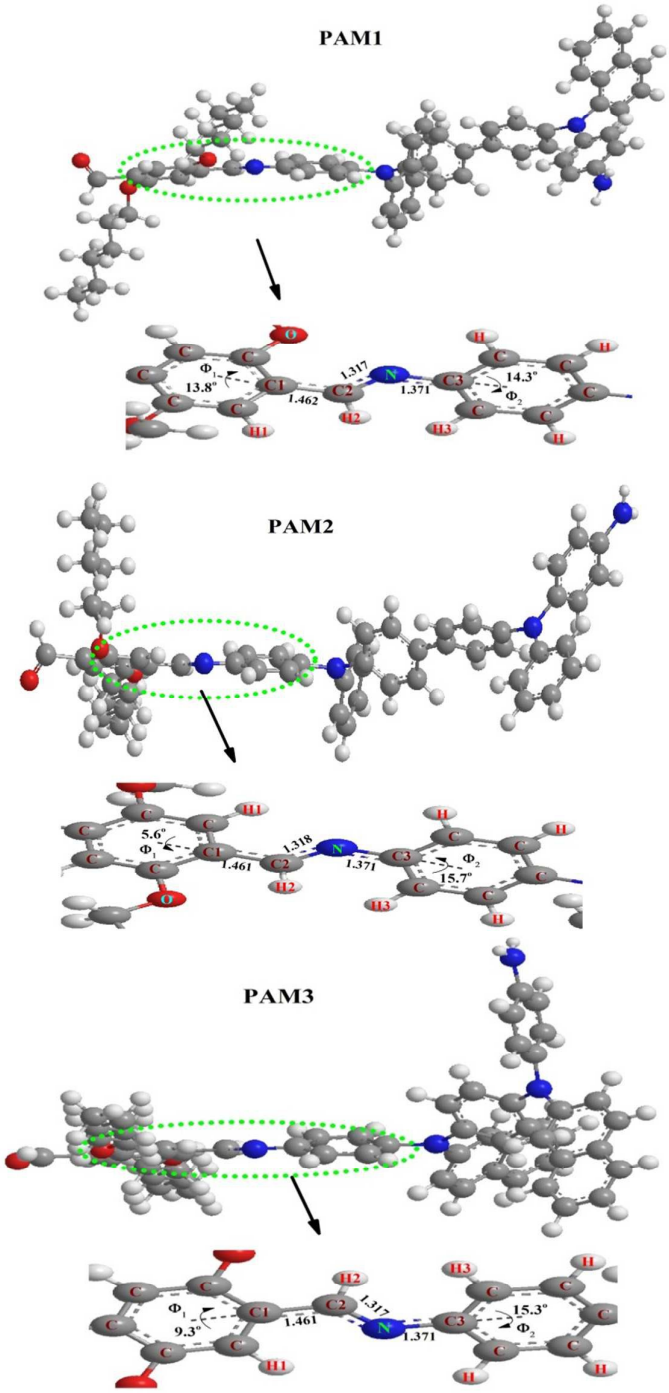

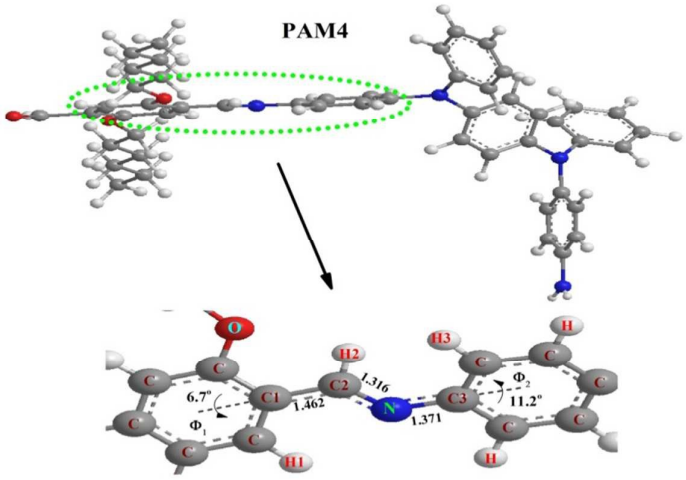

Fig.3. Optimized geometries of PAMs.

Fig. 4

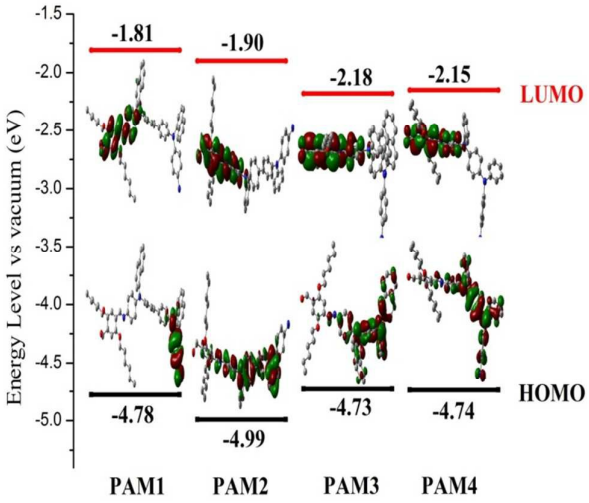

Fig.4. Pictorial representations of the electron density in the frontier molecular orbitals of repetition units.

Fig. 5

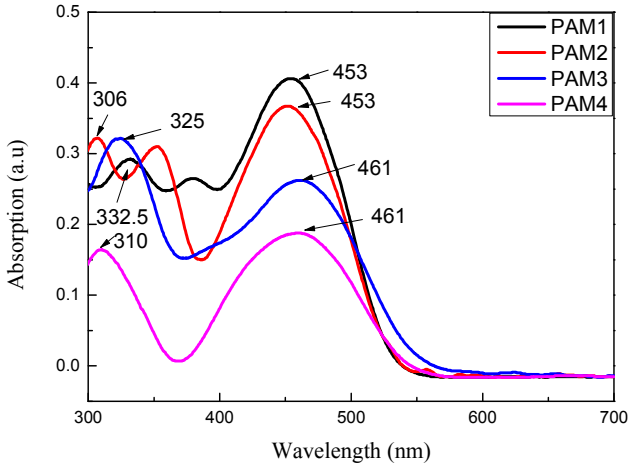

Fig.5. UV-visible absorption spectra of PAMs in CH_2Cl_2 at room temperature.

Fig. 6

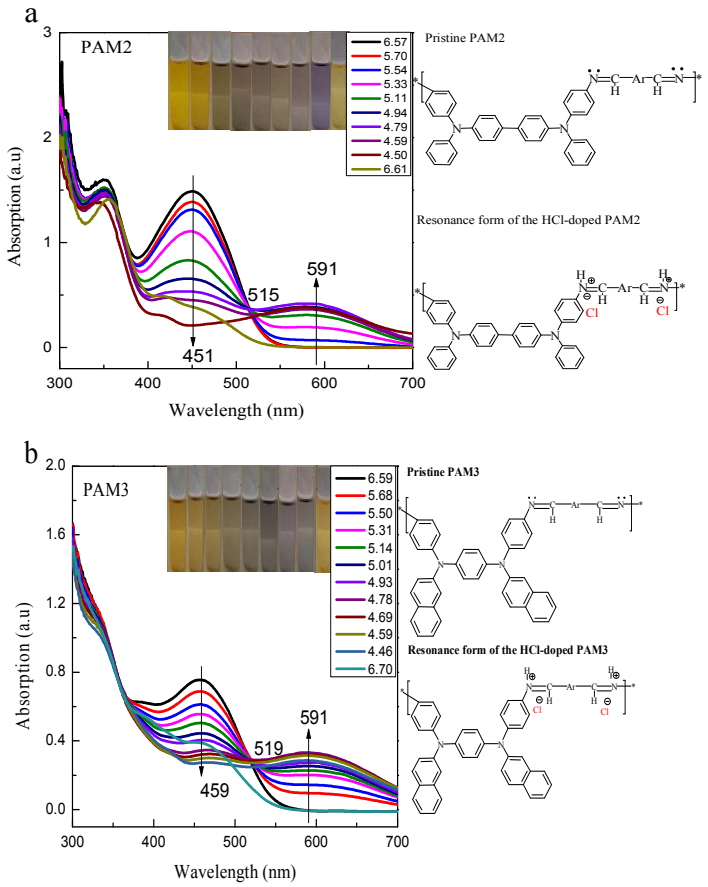

Fig.6. UV-vis spectra changes of PAM2 in the CH_2Cl_2 as they were protonated by HCl vapor in steps decrease with the value of pH decreasing. The concentration of pure PAMs was 0.03 mg/L. Inset photographs indicated the color evolved in the process of doping HCl vapor. The undoped molecular structure and protonated extreme resonance forms of PAMs shown on right.

Fig. 7

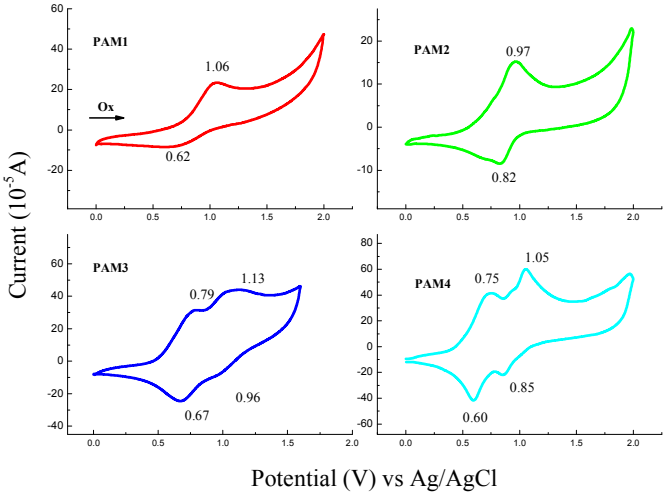

Fig.7. Cyclic voltammetry for PAMs in CH_3CN containing 0.1mol/L $LiClO_4$, at a scan rate of 50 mV/s.

Fig. 8

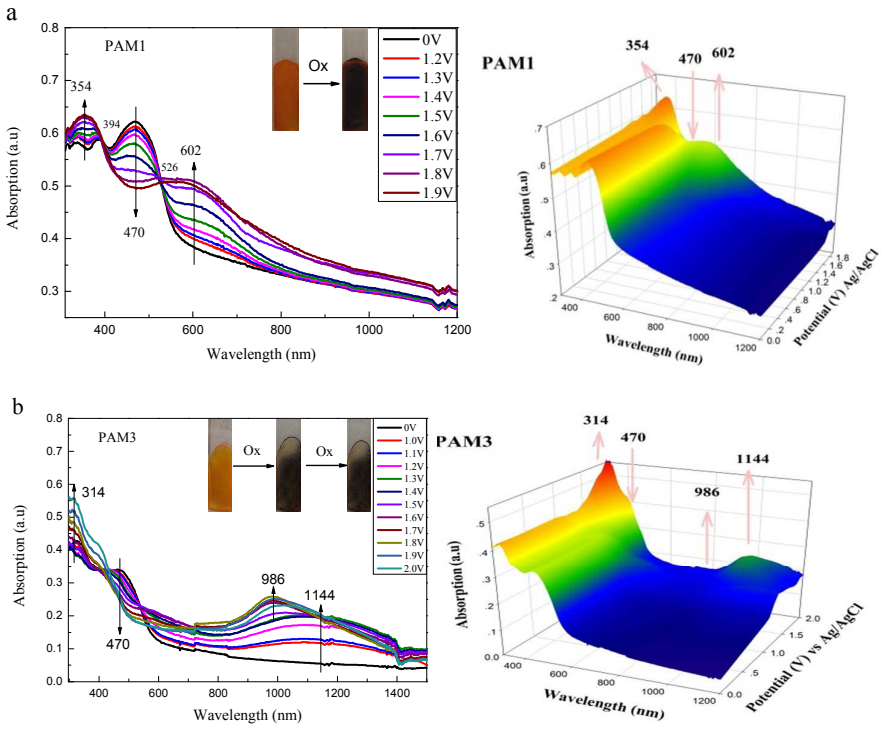

Fig.8. Electronic absorption spectra of films of PAM1 (a) and PAM3 (b) and their 3D spectra respectively, in the process of electrochemical doping with 0.1 V potential intervals in CH_3CN containing 0.1mol/L $LiClO_4$ as the supporting electrolyte (vs Ag/AgCl).

Fig. 9

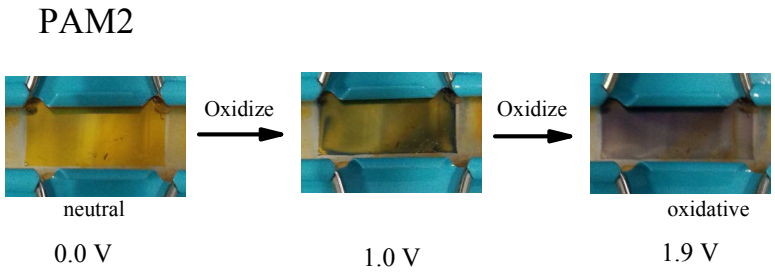

Fig.9. Electrochromic device of PAM2 containing 0.5mol/L $LiClO_4$ as the supporting electrolyte in the neutral (left) and oxidated (right) states.

Fig. 10

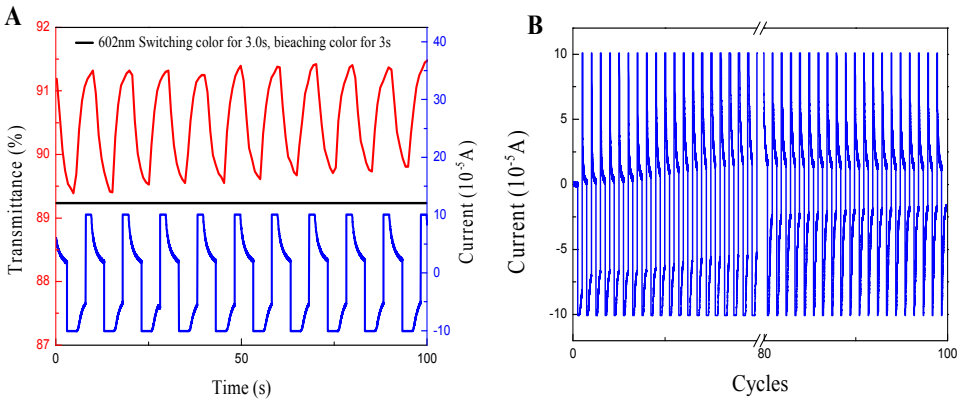

Fig.10. Potential step absorptiometry (A) and current consumption (B) of PAM1 at 602 nm (in 0.1 mol/L $LiClO_4/CH_3CN$) by applying a potential step (0.0-1.0 V) with a cycle time of 10 s.

Fig. 11

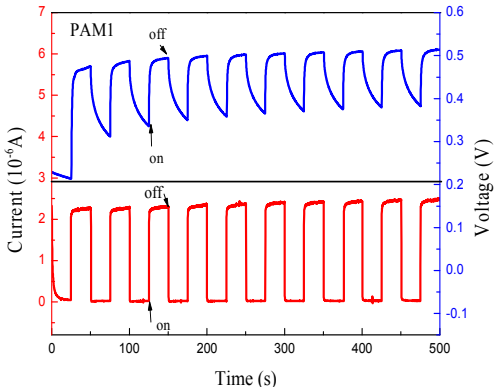

Fig.11. A typical photocurrent (lower) and photovoltaic (upper) response for an PAM1 film immobilized on ITO glass upon exposure to light with switching at room temperature.

Table 1

	5%	10%	20%	Char yield[a] wt%	M_w[b](g/mol)	M_n[b](g/mol)	PDI[c]
PAM1	400	420	450	53	36200	25400	1.43
PAM2	405	425	440	45	33800	24200	1.39
PAM3	400	420	440	41	32800	22500	1.44
PAM4	340	400	430	35	28500	21700	1.31

[a] The amount of carbonized residue of the polymers in the nitrogen atmosphere at 700 ^oC

[b] Calibrated with polystyrene standards, using THF as the eluent at a constant flow rate of 0.8 mL/min at 35 ^oC.

[c] Polydispersity index (M_w/M_n).

Table 1 Thermal properties and molecular weights of the PAMs.

Table 2

	$R_{C1\text{-}C2}$[a] Å	$R_{C2=N}$[a] Å	$R_{N\text{-}C3}$[a] Å	Φ_1[b] deg	Φ_2[b] deg	E_{HOMO} eV	E_{LUMO} eV	E_g eV
PAM1	1.462	1.317	1.371	13.8	14.3	-4.78	-1.81	2.94
PAM2	1.461	1.318	1.371	5.6	15.7	-4.99	-1.90	3.09
PAM3	1.461	1.317	1.371	9.3	15.3	-4.73	-2.18	2.55
PAM4	1.462	1.316	1.371	6.7	11.2	-4.74	-2.15	2.59

[a] $R_{C1\text{-}C2}$, $R_{C2=N}$, and $R_{N\text{-}C3}$ are defined in Figure 2. [b] Average value.

Table. 2. Calculated Bond Lengths, Dihedral Angles (Φ_1, Φ_2), and Electronic Structure (E_{HOMO}, E_{LUMO}, and E_g) of PAMs.

Table 3

	$\lambda_{solution}^{abs}$ (nm)[a]	λ_{film}^{abs} (nm)[b]	λ_{onset}^{abs} (nm)[b]	$E_{1/2}$ vs Ag/AgCl[c]	E_{onset}^{peak} vs Ag/AgCl	$E_{HOMO}^{electro}$ (eV)[e]	$E_{LUMO}^{electro}$ (eV)[e]	E_g^{film} (eV)[d]
PAM1	453	470	530	0.84	0.79	-5.14	-2.81	2.33
PAM2	453	456	534	0.90	0.60	-4.95	-2.63	2.32
PAM3	461	470	546	0.73	0.50	-4.85	-2.58	2.27
PAM4	461	466	552	0.68	0.44	-4.79	-2.54	2.25

[a] UV–vis absorption and PL spectra measurements in CH_2Cl_2 at room temperature.

[b] λ_{onset} of the polymer film.

[c] $E_{1/2}$: average potential of the redox couple peaks.

[d] $E = 1240/\lambda_{onset}$.

[e] The HOMO energy levels were calculated from cyclic voltammetry and were referenced to ferrocene (4.8 eV). $E_{LUMO} = E_{HOMO} + E_g$. $E_{ox/onset}$ (Fc/Fc vs Ag/AgCl) = 0.45 V.

Table 3. Optical and electrochemical properties for PAMs

Table 4

Polymer code[a]	$\lambda_{(nm)}$[b]	δ_{OD}[c]	Q(mC/cm^2)[d]	η(cm^2/C)[e]
PAM1	602	0.0092	0.044	208
PAM2	620	0.0014	0.008	172
PAM3	470	0.0034	0.042	78
PAM4	466	0.016	0.048	332

[a] Switching between 0.0 and 0.8 V for PAMs (V vs Ag/AgCl).

[b] The given wavelength where the data were determined.

[c] Optical density change at the given wavelength.

[d] Injected charge, determined from the in situ experiments.

[e] Coloration efficiency is derived from the equation $\eta=\delta_{OD}/Q$.

Table 4 Electrochemical data collected for coloration efficiency measurements of PAMs.